Journal of Applied Polymer Science

Morphological and Thermal Properties of Photodegradable Biocomposite Films

Sreejarani Kesavan Pillai,[1] Suprakas Sinha Ray,[1,2] Manfred Scriba,[1] Vincent Ojijo,[1] Mpitloane Joseph Hato[1]

[1]DST/CSIR National Centre for Nano-Structured Materials, Council for Scientific and Industrial Research, Pretoria 0001, South Africa

[2]Department of Applied Chemistry, University of Johannesburg, Doornfontein, 2028, South Africa

Correspondence to: S. K. Pillai (E-mail: skpillai@csir.co.za)

ABSTRACT: Biocomposites containing ultraviolet (UV) radiation absorbing inorganic nanofillers are of great interest in food packaging applications. The biodegradable polylactide (PLA) composite films were prepared by solvent casting method by incorporating 1 wt % of titanium dioxide (TiO_2) and Ag-TiO_2 (silver nanoparticles decorated TiO_2) nanoparticles to impart the photodegradable properties. The films were exposed to UV radiation for different time periods and morphology of the composite films before and after UV exposure were investigated. The results showed that homogenous filler distribution was achieved in the case of Ag-TiO_2 nanoparticles. The thermal properties and thermomechanical stability of the composite film containing Ag-TiO_2 nanoparticles were found to be much higher than those of neat PLA and PLA/TiO_2 composite films. The scanning electron microscopy and X-ray diffraction studies revealed that the photodegradability of PLA matrix was significantly improved in the presence of Ag-TiO_2 nanoparticles. © 2012 Wiley Periodicals, Inc. J. Appl. Polym. Sci. 129: 362–370, 2013

KEYWORDS: composites; degradation; nanoparticles; nanowires and nanocrystals; Biopolymers and renewable polymers

Received 25 September 2012; accepted 24 October 2012; published online 13 November 2012
DOI: 10.1002/app.38763

INTRODUCTION

Food packaging is one of the major fields of application for polymeric materials. Because of their nondegradable nature, there is an increasing desire for companies and consumers to reduce, recycle, and reuse plastic packaging materials, which are derived from traditional petrochemical-based polymers or, alternately, substitute them with environmentally friendly polymeric material, which is a more sustainable option.[1] Polylactide (PLA) derived from renewable resources, like corn, sugar beets, wheat, and other starch-rich products, is such a polymer that has shown huge potential to develop biodegradable plastics for textile, medical, and packaging industries.[2–4] However, neat PLA's inherent thermal and thermomechanical stability are not sufficient for a wide-range of applications.[5] Another important drawback of PLA is its slower decomposition under normal natural biodegradation conditions of ground moisture and bacteria.

Processing polymer composites with inorganic nanoparticles offers a great opportunity to enhance the physical, thermal, and mechanical properties of neat polymers.[6–8] The effectiveness of fillers with nanometric dimensions strongly depends on its shape, particle size, aggregate size, surface characteristics, and degree of dispersion.[9,10] According to the classical composite theory, improved interfacial bonding between polymer matrix and filler particles leads to enhance practical properties of the composites.[11]

PLA composites have been reported using various nanoparticles, including carbon nanotubes, layered silicates or clays, silica, graphite, magnesium oxide, and so forth.[2,3,8,12–15] Though these composites exhibited enhanced mechanical strength and modulus, very few nanoparticles could efficiently improve the thermal and thermomechanical stability of neat PLA.[13,16] This may be due to the lack of strong interfacial interactions between nanoparticles and PLA matrix.

Although the mechanical, physical, and thermal properties of PLA-based composites are important with respect to their in-house use and storage, ideally, these materials should biodegrade efficiently on disposal. Although biodegradation of polymers like PLA takes place at higher rates in compost where moisture and bacteria exist (it does not advance in air), more than three months is needed for the complete decomposition.[17] As an alternative strategy, by incorporating photodegradability

to a biodegradable polymer, the overall degradability can be efficiently improved under any conditions.[18–21]

Titanium dioxide (TiO_2) nanoparticles have been investigated in recent years because of the capability to absorb ultraviolet (UV) radiation ($\lambda < 388$ nm) and generate oxygen species[22,23] that decompose various organic chemicals such as aldehyde, toluene, and polymers such as polyethylene (PE),[24,25] polypropylene (PP),[26] poly(vinyl chloride) (PVC),[23] and polystyrene (PS).[27] It is well known that the photocatalysis reaction of TiO_2 produces active oxygen species such as O_2-, HO_2, and HO radicals from H_2O or O_2 by oxidative or reductive reactions under UV radiation exposures. These active oxygen species will lead to photodegradation reactions by attacking the interfacial polymer chains, forming carbon-centered radicals, and accelerating chain cleavage.[2,3]

Research in composites based on TiO_2 and PLA has recently been focused on applications like drug releasing,[5,28] degradation of organic pollutants,[4] and textiles.[29] A few studies have reported on improved dispersion of TiO_2 nanoparticles in PLA and the resulting PLA/TiO_2 composites' improved photodegradability. However, in these investigations, the TiO_2 nanoparticles used were surface modified by using tedious or multistep procedures to get good interfacial interaction with PLA matrix.[2,3,30–32] For example, Nakayama and Hayashi[3] reported improved photodegradability of PLA composites with TiO_2 nanoparticles modified by propionic acid and *n*-hexyl amine, independent of the filler content. Luo et al.[30] used functionalized TiO_2 with lactic acid through solution polycondensation reaction for the preparation of PLA/TiO_2 composites. Zhuang et al.[22] used organically modified TiO_2 to synthesize PLA/TiO_2 composites with improved mechanical and thermal properties by *in situ* polymerization.

Even though TiO_2 is a potential photocatalyst, the high rate of electron-hole recombination possibility sometimes results in low efficiency of photocatalysis.[33] Several studies have been recently reported on Ag modified TiO_2 for enhancing its photodegradation property.[34–36]

In this work, PLA composites were prepared by solvent casting method using Ag-modified TiO_2 without any further surface modification. This is compared to the structural and thermal properties of composites prepared by the same method but using TiO_2 nanoparticles. The effect of different nanofillers to the photodegradation property is also investigated. Low energy UV irradiation of 365 nm wavelength was chosen for the photodegradation study to create the UV exposure of natural environment. The powder samples and solvent casted composite films were characterized by X-ray diffraction (XRD), UV–visible spectroscopy (UV–vis), scanning electron microscopy (SEM), themogravimetric analysis (TGA), differential scanning calorimetry (DSC), and dynamic mechanical analyzer (DMA).

EXPERIMENTAL

Materials

PLA with a D-lactide content of 1.1–1.7% was obtained from Unitika, Japan. Prior to use, PLA was dried at 80°C for 2 h under vacuum. Commercial TiO_2 nanoparticles (P25) with diameter 20–40 nm were supplied by Degussa, Germany. The reagents such as, $CHCl_3$, NH_4OH, ethylene glycol (EG), and $AgNO_3$ were purchased from Sigma Aldrich and used as received without further purification.

Synthesis of Ag-TiO_2 Nanoparticles

In a typical synthetic procedure, 1 g of TiO_2 (P25, Degussa) was mixed with 100 mL of 0.01 M $AgNO_3$ solution and 10 mL EG, and magnetically stirred for 24 h at 60 °C. The solid mass was filtered, washed several times with distilled water, and finally dried in the oven at 110 °C overnight.

Preparation PLA/TiO_2 and PLA/Ag-TiO_2 Composite Films

PLA composite films with 1 wt % inorganic content (TiO_2 and Ag-TiO_2) were prepared by solvent-casting method. A known weight of PLA was dissolved in 100 mL $CHCl_3$ by ultrasonication. The inorganic oxide was added to the PLA solutions and magnetically stirred for 2 h at room temperature. The mixture was then poured into Petri dishes, and the solvent was allowed to evaporate overnight. The films were peeled off from the Petri dishes and annealed at 80°C overnight under vacuum. Neat PLA film was also prepared under the same conditions for comparison.

Characterization of TiO_2 and Ag-TiO_2 Powder Samples

The nanoparticle size and shape were analyzed by a JEOL 2100 TEM, operated at 200 kV. To prepare the sample for TEM, the powder was sonicated in methanol for 5 min, followed by depositing the solution on a Cu-grid with holey carbon film. The UV–vis characteristics of the nanoparticles were recorded by a Perkin-Elmer Lambda 750 UV–vis spectrometer. The SEM analysis was done using a JEOL 7500 SEM at an accelerating voltage of 5 kV. Elemental analysis was performed using a NORAN EDS system, which was attached to the JEOL 7500 SEM.

Characterization of PLA and its TiO_2 or Ag-TiO_2 Containing Composite Films

The following techniques were used to characterize neat PLA and the corresponding composite films before and after UV exposure. DSC investigations were performed by means of a DSC Q2000 (TA Instruments) in nitrogen atmosphere at a flow rate of 50 mL/min. The samples were sealed in aluminum pans. To study the effect of incorporation of filler on cold crystallization behavior of PLA, all samples were heated from 25 to 200°C at a rate of 5°C/min, annealed for 5 min at 200°C to erase previous thermal history, cooled down to 25°C at 5°C/min, and then repeated heating scanned immediately to 200°C at a rate of 5°C/min. The crystallization peak (T_c) and melting peak (T_m) temperatures, and the degree of crystallization (χ_c) were determined from the thermograms. χ_c was calculated according to the relation $\chi_c = [\Delta H_m/\omega\Delta H_f] \times 100$, where ω is the weight fraction of PLA component, ΔH_m is the enthalpy of melting and ΔH_f is the heat of fusion of 100% crystalline PLA (taken as 93 J g^{-1}).[37] To study the effect of filler on PLA T_g, annealed samples (at 80°C for overnight under vacuum) were equilibrated at −25°C for 30 min and then heated to 200°C at a rate of 20°C/min. A field-emission SEM (JEOL 7500 FESEM) was used to characterize the surface morphology of the neat PLA and composite films. The XRD analyses were conducted on a PANalytical XPERT-PRO diffractometer using Ni-filtered CuKα radiation ($\lambda = 1.5406$ Å) with a fixed slit at 45 kV (voltage) and 40 mA (current) in the diffraction angle range of 2–80°C.

Applied Polymer SCIENCE

The thermal stability of the neat PLA and two different composite films was investigated by thermogravimetric analyzer using a Q500 TGA instrument in a normal air environment. The samples were heated in platinum crucibles with an air flow of 50 mL/min. The dynamic measurement was conducted from ambient temperature to 900°C, with a ramp rate of 10°C/min. The dynamic mechanical analysis of neat PLA and two different composite samples were examined by means of Perkin Elmer DMA 8000 in a single cantilever mode with a pocket material. To measure the thermomechanical stability of neat PLA, before and after composites formation, the temperature sweep experiments were conducted at a constant strain amplitude of 0.02% (calculated after series of experiments) and frequency of 6.28 rad s^{-1} (1 Hz). The heating rate was 2°C/min over the range of −25–175°C.

Degradation Study Under UV Radiation

Annealed neat PLA and composite films were cut into rectangles (1 × 4 cm^2) and mounted on glass plates. The samples were then exposed to UV monochromatic radiation (λ = 365 nm) in a UV chamber for two irradiation intervals of 8 and 16 h (sample notation, e.g., PLA′ and PLA*) at room temperature. The distance between the UV lamp and the sample was 15 cm at an intensity of 950 μW cm^{-2}. The estimated total radiant exposures were 27.3 and 54.7 J cm^{-2} for 8 and 16 h, respectively.

RESULTS AND DISCUSSION

Morphology and Structure of TiO_2 and Ag-TiO_2 Nanoparticles

Parts (a) and (b) of Figure 1 show the TEM images of TiO_2 and Ag-TiO_2, respectively. The TiO_2 has a grain distribution of 20–50 nm and typically the exposed surfaces are smoother [refer to Figure 1(a)]. The TEM image of Ag-TiO_2 presented in Figure 1(b) shows uniform distribution of Ag nanoparticles with a mean diameter less than 5 nm, on the surface of TiO_2 particles. One could clearly notice the change in the surface morphology, that is, increased surface roughness of the TiO_2 nanoparticles due to the deposition of Ag.

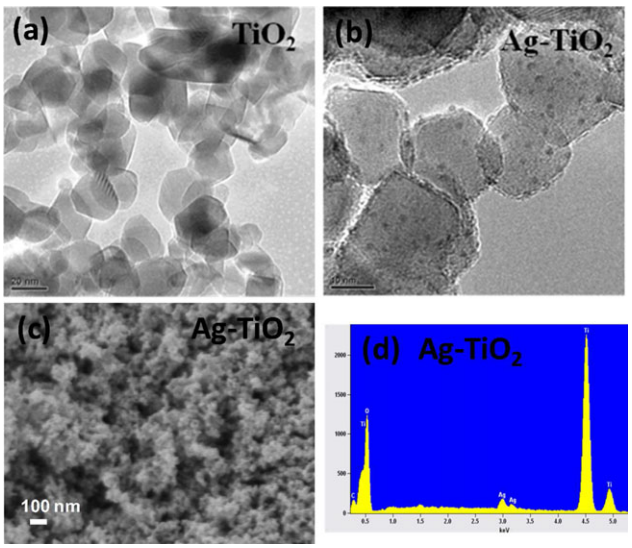

Figure 1. Bright field transmission electron microscopic image of (a) TiO_2 and (b) Ag-TiO_2 nanoparticles. (c) Field-emission scanning electron microscopic image of Ag-TiO_2 nanoparticles and (d) corresponding energy-dispersive X-ray spectrum. [Color figure can be viewed in the online issue, which is available at wileyonlinelibrary.com.]

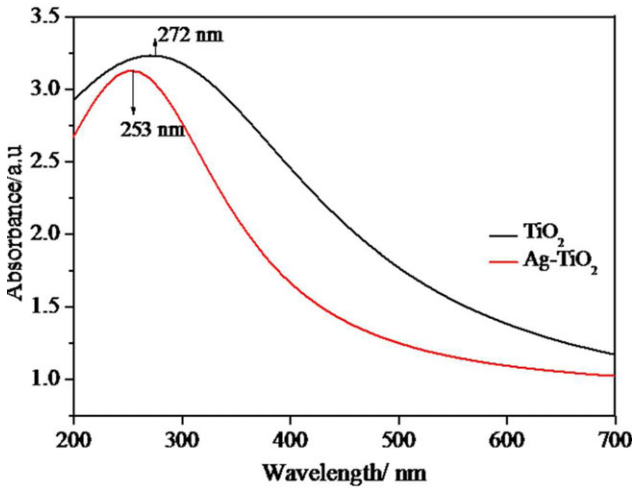

Figure 2. UV–vis absorption spectra of TiO_2 and Ag-TiO_2 nanoparticles. [Color figure can be viewed in the online issue, which is available at wileyonlinelibrary.com.]

The FESEM image of Ag-TiO_2 sample and its EDS spectrum is shown in Figure 1(c). TiO_2 nanoparticles with particle sizes in the 20–50 nm can be seen in the SEM micrograph. Though, the presence of Ag nanoparticles on the TiO_2 surface is not clearly visible from the micrograph, the EDS spectrum [refer to Figure 1(d)] shows the characteristic signals of Ti, O, and Ag confirming the successful incorporation of Ag into TiO_2 and the high purity of the synthesized material. The average concentration of Ag on TiO_2 obtained from multispot analysis is close to 3.95 wt % (1.3 atm %).

The UV–vis spectra of TiO_2 and Ag-TiO_2 nanoparticles are shown in Figure 2. A broad band absorption ranging from 250 to 350 nm is observed for both samples. However, it is noteworthy that Ag-TiO_2 sample shows an absorption band, upward shifted (blue shifted) relative to that of TiO_2 nanoparticles. The

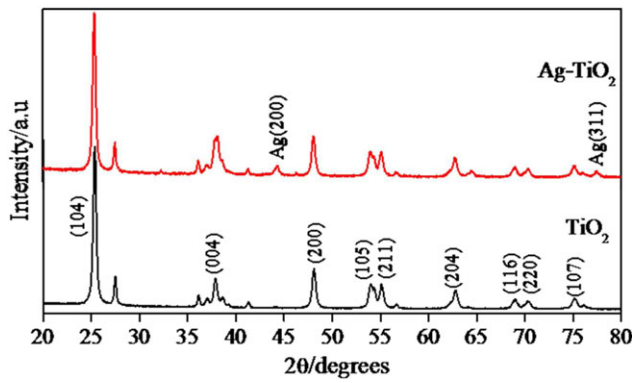

Figure 3. XRD patterns of TiO_2 and Ag-TiO_2 nanoparticles. [Color figure can be viewed in the online issue, which is available at wileyonlinelibrary.com.]

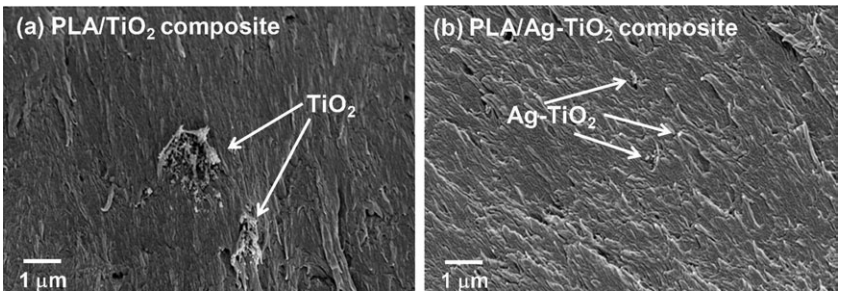

Figure 4. Field-emission SEM fractured-surface image of (a) PLA/TiO_2 and (b) PLA/Ag-TiO_2 composite films.

blue shift is ascribed to a phenomenon known as quantum confinement effect, whereas in the case of nanoparticles with much smaller size; the optical edge tends to shift to higher energy.[38,39] In the case of Ag-TiO_2 sample, the blue shift is due to the presence of additional, very small sized Ag nanoparticles on the TiO_2 surface.

The XRD patterns in Figure 3 show tetragonal anatase as the predominant crystalline phase of TiO_2 in both TiO_2 and Ag-TiO_2 samples (reference code: 01-075-1537). The Ag-TiO_2 sample shows less intense additional peaks at 2θ = 44.4 and 77.2°C, confirming the presence of a cubic phase of Ag nanoparticles (reference code: 00-003-09210).

Fractured Surface Morphology of Composite Films

The TiO_2 and Ag-TiO_2 nanoparticle distribution and the presence of their aggregates in PLA matrix were studied with FESEM. Parts (a) and (b) of Figure 4 show the fractured-surface morphology of PLA/TiO_2 and PLA/Ag-TiO_2 composite films, respectively. PLA loaded with 1 wt % Ag-TiO_2 shows a reasonably good degree of dispersion with fewer tendencies of nanoparticles for aggregation when compared to PLA/TiO_2 composite containing the same amount of TiO_2 loading. The surface roughness of the polymer observed in PLA/TiO_2 is higher with respect to PLA/Ag-TiO_2 indicating a higher degree of nanoparticle aggregation in the case of PLA/TiO_2 composite film. The SEM micrograph of PLA/Ag-TiO_2 also shows well-embedded Ag-TiO_2 nanoparticles with no pull-outs during fracture, illustrating strong binding between the Ag-TiO_2 and the PLA matrix. This may be due to the very rough surface of Ag-TiO_2 nanoparticles (refer to the TEM images in Figure 1), which leads to the strong adsorption of PLA chains on Ag-TiO_2 surface. We will confirm this as we progress.

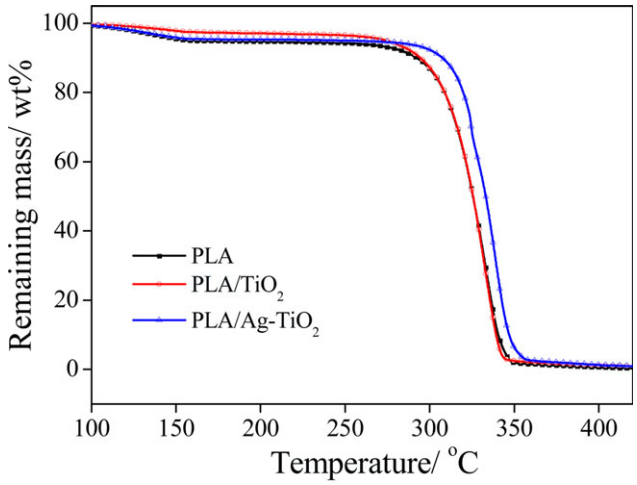

Figure 5. Thermogravimetric scans of neat PLA and two different composite films under air. [Color figure can be viewed in the online issue, which is available at wileyonlinelibrary.com.]

Thermal Stability

The TGA scans for neat PLA and two different composite samples (PLA/TiO_2 and PLA/Ag-TiO_2) are presented in Figure 5. Table I shows the onset decomposition temperature (at 5% weight loss), the temperature at 10% weight loss, and char yield (at 600°C) for the samples. The initial decomposition temperature of neat PLA is 263°C (at 5% weight loss), which is significantly shifted to a higher value for PLA/Ag-TiO_2 composite (290.1°C), whereas the value is decreased in the case of PLA/TiO_2 composite film (261.5°C) as compared to neat PLA film. This may be due to the poor adhesion of TiO_2 smooth surfaces to the PLA matrix.[2,3] Furthermore, the higher thermal stability of PLA/Ag-TiO_2 composite could be attributed to a good dispersion of Ag-TiO_2 nanoparticles in PLA matrix. According to the TEM images (refer to Figure 1), Ag-TiO_2 nanoparticles have rough surfaces, which lead to better adsorption of PLA chains on Ag-TiO_2. Another reason may be the presence of higher thermally stable Ag nanoparticles in Ag-TiO_2, which contribute to the enhancement of the overall thermal stability of PLA/Ag-TiO_2 composite. The residue obtained at 600°C for neat PLA is 0.03% while those of composites are in the range 0.8–0.9%.

Thermal Properties

Figure 6(a) shows the DSC thermograms of annealed neat PLA and composite films. Figure 6(b) shows the DSC thermograms of neat PLA and the composites after erasing the previous

Table I. Data Calculated from TGA Analysis

Films	T_d^{onset} (°C)	$T_d^{10\%}$ (°C)	Residue at 600°C (%)
PLA	263.7 ± 0.68	290.7 ± 0.51	0.03 ± 0.02
PLA/TiO_2 composite	261.5 ± 1.70	293.8 ± 0.67	0.92 ± 0.03
PLA/Ag-TiO_2 composite	290.1 ± 0.78	306.1 ± 1.62	0.84 ± 0.11

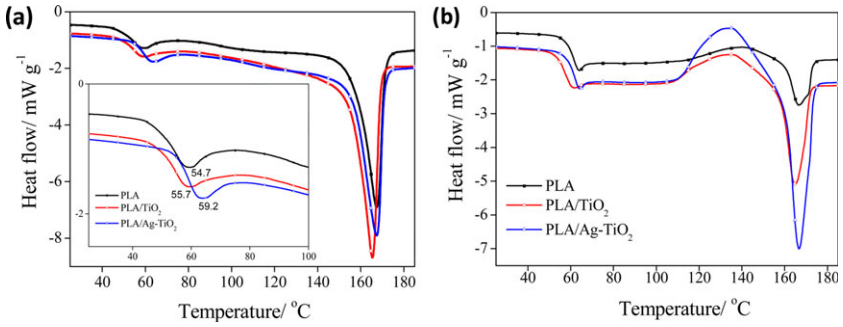

Figure 6. DSC thermograms of neat PLA and the composite films: (a) annealed samples, first runs and (b) from second runs. [Color figure can be viewed in the online issue, which is available at wileyonlinelibrary.com.]

thermal history, and the parameters determined from these DSC scans are tabulated in Table II. The following features are observed, mainly:

i. The T_g for all samples is seen clearly [refer to Figure 6(a)]. Such an observation indicates all samples are constraint free after annealing at 80°C overnight. The T_g of neat PLA (54.7°C) is slightly increased in the case of the PLA/TiO_2 (55.7°C) composite. This may be due to the unfavorable interaction between PLA matrix and TiO_2 particles, while the T_g of neat PLA is significantly improved in the case of PLA/Ag-TiO_2 composite film. This is quite unusual in the case of PLA-based composite. We believe this may be due to the strong adsorption (or physical interaction) of PLA macromolecules on the rough Ag-TiO_2 surface.
To gain insight into possible interaction of fillers with PLA, FT-IR spectra of the neat polymer and composites were recorded in the range of 550–4000 cm^{-1}(refer to Figure 7). The peak positions for PLA in the spectra of composites remained unaltered indicating the absence of any chemical interaction between the PLA matrix and Ag-TiO_2 nanoparticles. Such an observation indicates further in depth study is necessary to understand the interfacial interactions between Ag-TiO_2 nanoparticles and PLA matrix.

ii. A sharp cold-crystallization peak appears for all samples. Such a result indicates that, for all samples, the cold crystallization process of PLA matrix takes place from a single homogeneous phase. However, it is interesting to note that the cold crystallization peak temperature of neat PLA moves toward much lower temperatures in the case of composites, and it is significant in the case of PLA/Ag-TiO_2 composite. This indicates an efficient nucleating role of the Ag-TiO_2 nanoparticles for PLA crystallization. We believe this is due to the homogeneous dispersion of Ag-TiO_2 nanoparticles in the PLA matrix, which consequently act as nucleators of the PLA chains to fold and join the crystallization growth front efficiently. This is supported by the higher overall crystallinity of PLA/Ag-TiO_2 composite (refer to Table II).

iii. The melting peak temperature (corresponding to the main peak) of the composites shifts to the lower temperature region than that of neat PLA, and this effect is more prominent in the case of the PLA/Ag-TiO_2 composite [refer to Figure 6(b)]. Such results indicate the formation of much smaller or less perfect crystallites in the case of composites than neat PLA. The appearance of double melting peaks in the case of composites suggests the presence of two different types of thermally stable PLA crystallites; however, there is a significant difference in population.

Thermomechanical Stability

The temperature dependence of tan δ of neat PLA and composites are presented in Figure 8. The temperature of maximum tan δ of neat PLA film is generally considered as matrix T_g (66.3°C), which is slightly affected by incorporation of TiO_2 nanoparticles in the case of PLA/TiO_2 composite. However, this improvement is significant in the case of PLA/Ag-TiO_2 composite film. Such a unique observation in the case of Ag-TiO_2 nanoparticle-containing composite of PLA supports strong adsorption of PLA chains on rough Ag-TiO_2 surfaces. This lead to the immobilization of PLA chains, and, hence, enhanced thermomechanical properties. However, further study needs to be performed to find out the specific reason for this improvement in thermomechanical stability of PLA/Ag-TiO_2 composite.

Crystalline Structure

The crystalline structure of neat PLA before and after composite preparation was studied using XRD. The XRD patterns of

Table II. Thermal Properties of Neat PLA and Two Different Composite Films

Films	T_g (°C)	T_c (°C)	T_m (°C)	ΔH_m (J g^{-1})	χ_c (%)
PLA	54.7 ± 0.55	140.1 ± 1.10	166.6 ± 0.43	6.8 ± 0.35	7.3 ± 0.36
PLA/TiO_2 composite	55.7 ± 0.95	135.3 ± 1.05	164.6 ± 0.91	15.02 ± 1.23	16.5 ± 0.58
PLA/Ag-TiO_2 composite	59.2 ± 0.62	134.1 ± 0.85	164.3 ± 1.05	25.1 ± 0.95	27.9 ± 1.06

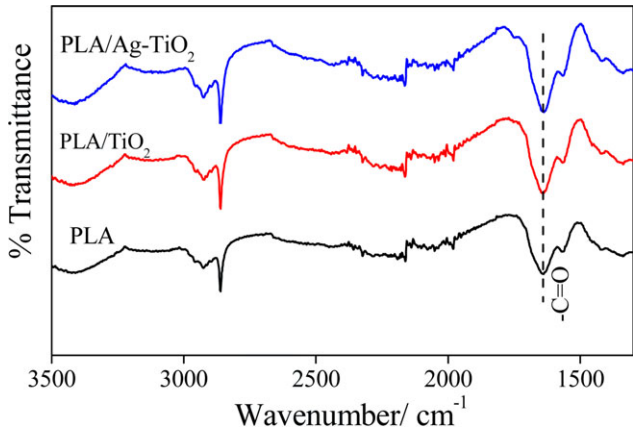

Figure 7. Fourier-transform infrared spectra of neat PLA and composite films. [Color figure can be viewed in the online issue, which is available at wileyonlinelibrary.com.]

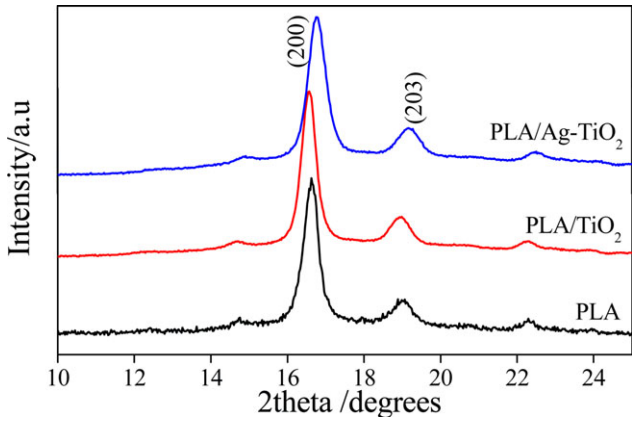

Figure 9. XRD patterns of annealed neat PLA and composite films. [Color figure can be viewed in the online issue, which is available at wileyonlinelibrary.com.]

annealed neat PLA and the composites are shown in Figure 9. It can be seen that the neat PLA film exhibits a very strong peak at $2\theta = 16.8°$ due to reflection from (200) and/110 planes, and another less intense peak at $2\theta = 19.5°$ coming from the (203) plane. These peaks are assigned to the reflection of α-phase crystallite of PLA, which is orthorhombic with chains in a $-10/3$ helical conformation.[40] In the case of PLA/TiO_2 composite film, these characteristic peaks of the PLA matrix appear almost at the same positions, while both peaks are slightly up-shifted in the case of PLA/Ag-TiO_2 composite film. Such an observation indicates that PLA matrix crystallized in a defect-ridden form in the case of PLA/Ag-TiO_2 composite. This type of growth of PLA crystallites may be due to the homogeneous dispersion of Ag-TiO_2 nanoparticles in PLA/Ag-TiO_2 composite film.

Photodegradation

To study the photodegradation, neat PLA and its composite films containing TiO_2 and Ag-TiO_2 nanoparticles were exposed to UV radiation (wave length, $\lambda = 365$ nm) for two different time intervals of 8 and 16 h, thereafter, the films surface

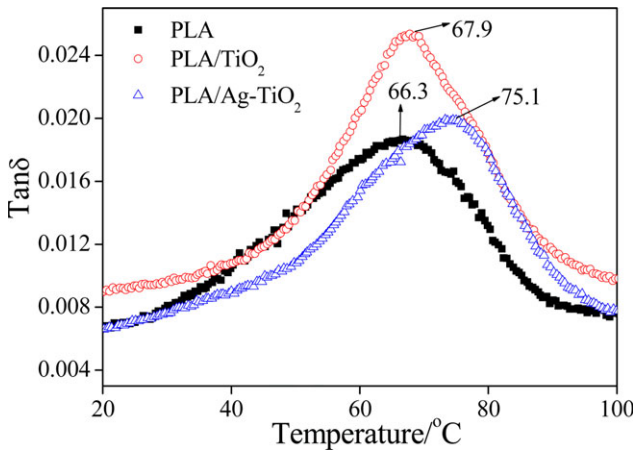

Figure 8. Temperature dependence of tan δ of neat PLA and composite films. [Color figure can be viewed in the online issue, which is available at wileyonlinelibrary.com.]

morphology and crystalline structure of PLA were respectively analyzed using SEM and XRD. From the SEM images shown in Figure 10, it is clear that the degradation of neat PLA film gradually increases with increased UV exposure time as indicated by the number of small cracks on the PLA surface. In the case of PLA/TiO_2 composite film, the degradation rate is initially higher but decreases with higher exposure time. As TiO_2 nanoparticles have the ability to absorb the UV radiation, it seems that they suppress the photodegradation and protect the remaining PLA surface when TiO_2 nanoparticles were directly exposed to the UV radiation after degradation of matrix. Nakayama and Hayashi[3] reported similar observations on PLA films containing a higher amount (~10 wt %) of TiO_2.

Conversely, the PLA composite film filled with Ag-TiO_2 nanoparticles shows the highest degradation rate among all the films, which significantly improves after 16 h of UV exposure. The surface of the composite is obviously degraded to a greater extent, with a noticeable increase in the size of the cavities (refer to Figure 10).

The XRD patterns of neat PLA and composite films after UV exposure, at two different times, are given in Figure 11. The increase degradation rate of PLA matrix with exposure time is reflected by the splitting of the main crystalline peak of PLA matrix after 16 h of UV irradiation. The efficient degradation rate in PLA/Ag-TiO_2 composite, when compared to PLA/TiO_2 film, is clearly seen from the significant reduction in the peak intensity of PLA as a result of efficient photodegradation. The split XRD peak is observed from 8 h of UV exposure in this case. This result also indicates that the Ag content on the TiO_2 surface is within the range of maximum photonic efficiency (1.5 atm %-optimum Ag loading).[41]

It is well reported that noble metals like Pt,[42] Au,[43] or Ag[44] deposited TiO_2 have high Schottky barriers and thus act as electron traps, facilitating electron-hole separation and promote an interfacial electron transfer process.[45,46] In this case, Ag nanoparticles accept the electrons formed on TiO_2 surface under UV radiation thereby reducing the electron-hole pair recombination, and transfer them to oxygen forming active oxygen species (refer to Scheme 1).[47] The active oxygen species initiate the

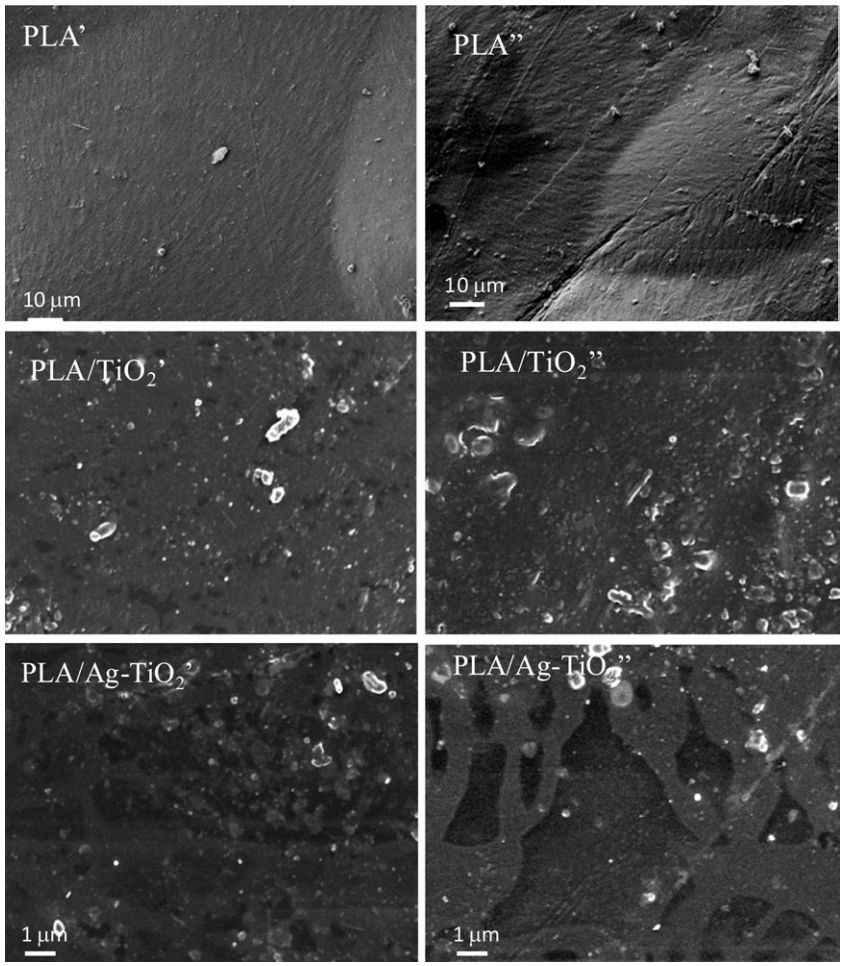

Figure 10. Field-emission scanning electron microscopic images of PLA and the composite films after UV exposure for 8 (′) and 16 h (″).

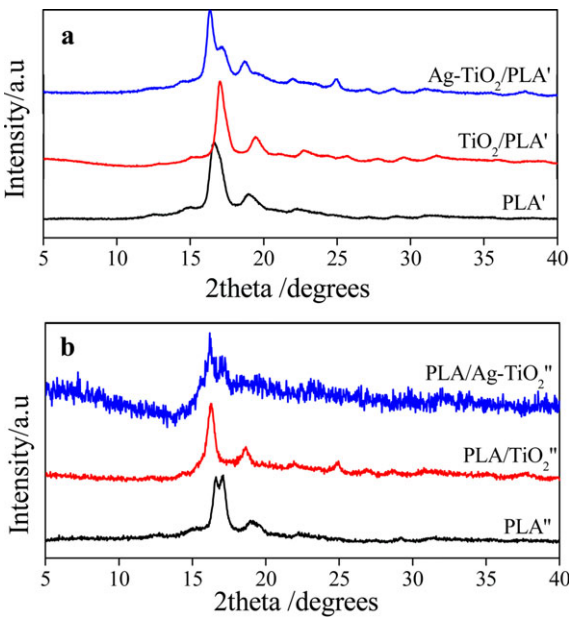

Figure 11. XRD pattern of neat PLA and the composite films after UV exposure: (a) 8 h and (b) 16 h. [Color figure can be viewed in the online issue, which is available at wileyonlinelibrary.com.]

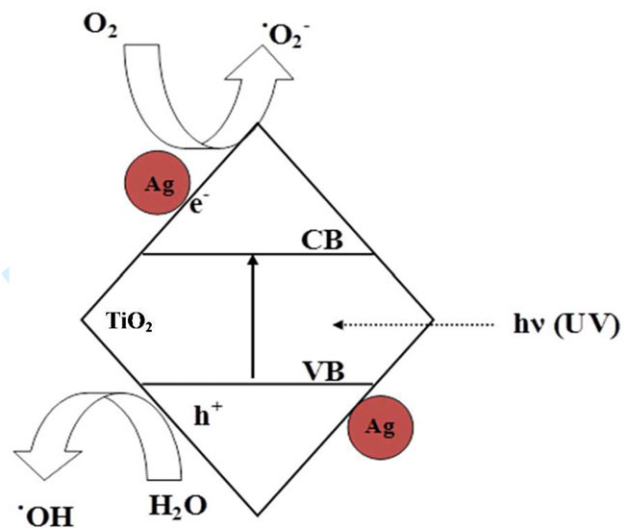

Scheme 1. Pathway of charge transfer in Ag-TiO_2 under UV irradiation (VB- valence band, CB-conduction band). [Color figure can be viewed in the online issue, which is available at wileyonlinelibrary.com.]

degradation by attacking the interfacial PLA chains, and this process is extended to the matrix through diffusion of reactive oxygen species.[2,3] This phenomenon describes the more efficient and faster degradation of PLA/Ag-TiO_2 nanocomposite film in comparison to PLA/TiO_2 under UV irradiation.

CONCLUSIONS

The TiO_2 and Ag-TiO_2 nanoparticles, without any further surface modification, were successfully incorporated as fillers in biodegradable PLA matrix by solvent casting technique. The overall thermal stability of the PLA composite film containing Ag-TiO_2 was found to be much higher than that of neat PLA and PLA/TiO_2 composite films. The overall degree of crystallinity and thermomechanical stability of PLA matrix was significantly increased for PLA/Ag-TiO_2. The photodegradation rate of PLA was also drastically enhanced by incorporating Ag-TiO_2 nanofillers. All these results are attributed to the homogenous dispersion of Ag-TiO_2 nanoparticles in PLA matrix. The Ag nanoparticles on TiO_2 surface play an important role in increasing the surface roughness of TiO_2 nanoparticles for better interaction with the PLA matrix as well as for the overall UV degradation ability of the resultant composite. In our ongoing research, we are trying to fine tune the size of Ag-TiO_2 nanoparticles in such a way that they can absorb light in the visible region. We are also diligently working to understand the interfacial interactions between Ag-TiO_2 nanoparticles and PLA matrix.

ACKNOWLEDGMENTS

The authors thank the Department of Science and Technology and the Council for Scientific and Industrial Research, South Africa, for the financial support.

REFERENCES AND NOTES

1. Piringer, O.; Baner, A. Plastic Packaging, 2nd ed.; Wiley-VCH Velag GmbH & Co. KGaA, **2008**; p 2.
2. Ojijo, V.; Sinha Ray, S.; Sadiku, R. ACS *Appl. Mater. Interfaces* **2012**, *4*, 2395.
3. Nakayama, N.; Hayashi, T. Polym. *Degrad. Stab.* **2007**, *92*, 1255.
4. Zhu, Y.; Buonocor, G. G.; Lavorgna, M.; Ambrosio, L. Polym. *Comp.* **2011**, *32*,435.
5. Sinha Ray, S.; Bousmina, M. *Prog. Mater. Sci.* **2005**, *50*, 962.
6. Chen, C.; Lv, G.; Pan, C.; Song, M.; Wu, C.; Guo, D.; Wang, X.; Chen, B.; Gu, Z. Biomed. *Mater.* **2007**, *2*, L1.
7. Paul, D. R.; Robeson, L. M. *Polymer* **2008**, *49*,3187.
8. Sinha Ray, S.; Maiti, P.; Okamoto, M.; Yamada, K.; Ueda, K. *Macromolecules* **2002**, *35*, 3104.
9. Curtin, W. A.; Sheldon, W. B. Mater. *Today* **2004**, *7*, 44.
10. Chan, C. M.; Wu, J.; Li, J. X.; Cheung, Y. K. *Polymer* **2002**, *43*, 2981.
11. Ciprai, D.; Jacob, K.; Tannenbaum, R. *Macromolecules* **2006**, *39*, 6565.
12. Nam, J. Y.; Sinha Ray, S.; Okamoto, M. *Macromolecules* **2003**, *36*, 7126.
13. Wu, C. S.; Liao, H. T. *Polymer* **2007**, *48*, 4449.
14. Song, W.; Zheng, Z.; Tang, W.; Wang, X. *Polymer* **2007**, *48*, 3658.
15. Yan, S.; Yin, J.; Yang, Y.; Dai, Z.; Ma, J.; Chen, X. *Polymer* **2007**, *48*, 1688.
16. Tsuji, H.; Takai, H.; Saha, S. K. *Polymer* **2006**, *47*, 3826.
17. Shogren, R. L.; Doane, W. M.; Garlotta, D.; Lawton, J. W.; Willett, J. L. Polym. *Degrad. Stab.* **2003**, *79*, 405.
18. Ikada, E. J. J. Photopolym. *Sci. Technol.* **1997**, *10*, 265.
19. Ikada, E. J. J. Photopolym. *Sci. Technol.* **1998**, *11*, 23.
20. Copinet, A.; Bertrand, C.; Govindin, S.; Coma, V.; Couturier, Y. *Chemosphere* **2004**, *55*, 763.
21. Copinet, A.; Bertrand, C.; Longieras, A.; Coma, V.; Couturier, Y. J. Polym. *Environ.* **2003**, *11*, 169.
22. Zhuang, W.; Liu, J.; Zhang, J. H.; Hu, B. X.; Shen, J. J. Polym. *Compos.* **2009**, *30*, 1074.
23. Zan, L.; Wang, S.; Fa, W.; Hu, Y.; Tian, L.; Deng, K. *Polymer* **2006**, *47*, 8155.
24. Ohtani, B.; Adzuma, S.; Nishimoto, S. I.; Kagiya, T. Polym. *Degrad. Stab.* **1992**, *35*, 53.
25. Zan, L.; Fa, W.; Wang, S. Environ. *Sci. Technol. 2006*, 40, **1681**.
26. Ohtani, B.; Adzuma, S.; Miyadzu, H.; Nishimoto, S. I.; Kagiya, T. Polym. *Degrad. Stab.* **1989**, *23*, 271.
27. Kim, S. H.; Kwak, S. Y.; Suzuki, T. *Polymer* **2006**, *47*, 3005.
28. Song, M.; Pan, C.; Chen, C.; Li, J.; Wang, X.; Gu, Z. *Appl. Surf. Sci.* **2008**, *255*, 610.
29. Carneiro, J. O.; Teixeira, V.; Nascimento, J. H. O.; Neves, J.; Tavares, P. B. J. Nanosci. *Nanotechnol.* **2011**, *11*, 1–8.
30. Luo, Y. B.; Li, W. D.; Wang, X. L.; Xu, D. Y.; Wang, Y. Z. Acta Mater. **2009**, *57*, 3182.
31. Luo, Y. B.; Wang, X. L.; Xu, D. Y.; Wang, Y. Z. *Appl. Surf. Sci.* **2009**, *255*, 6795.
32. Nakayama, N.; Hayashi, T. Colloids Surfaces A: Physicochem. *Eng. Asp.* **2008**, *317*, 543.
33. Linsebigler, A.;Lu, G.;Yates, J. T. *Chem. Rev.* **1995**, *95*, 735.
34. Mirkhani, V.; Tangestaninejad, S.; Moghadam, M.; Habibi, M. H.; Rostami-Vartooni, A. J. *Iran. Chem. Soc.* **2009**, *6*, 578.
35. Behpour, M.; Ghoreishi, S. M.; Razavi, F. S. Digest J. Nanomater. *Biostruct.* **2010**, *5*, 467.
36. Liang, W.; Li, J.; Jin, Y. Building Environ. **2012**, *51*, 345.
37. Fischer, E. W.; Sterzel, H. J.; Wegner, G. *Kolloid-Zeitschrift & Zeitschrift for Polymere* **1973**, *251*, 980.
38. Mao, Y.; Wong, S. S. J. *Am. Chem. Soc.* **2006**, 128, 8217.
39. Cesano, S. B. F.; Uddin, M. J.; Agostini, G.; Scarano, D.; Zecchina, A. J. *Phys. Chem. C* **2010**, *114*, 169.

40. Schmidt, S. C.; Hillmyer, M. A. J. Polym. *Sci. Part B: Polym. Phys.* **2001**, *39*, 300.

41. Herrmann, J. M.; Disdier, J.; Pichat, P.; Malato, S.; Blanco, J. *Appl. Catal. B: Environ.* **1998**, *17*, 15.

42. Li, Y.; Chen, C.; Li, J.; Sun, X. S. *Polymer* **2011**, *52*, 2367.

43. Buzarovska, A.; Grozdanov, A. J. *Appl. Polym. Sci.* **2011**, *123*, 2187.

44. Brizzolara, D.; Cantow, H. J.; Diederichs, K.; Keller, E.; Domb, A. J. *Macromolecules* **1996**, *29*, 191.

45. Sclafani, A.; Palmisano, L.; Marcil, G.; Venezia, A. M. Solar Energy Mater. *Solar Cells* **1998**, *51*, 203.

46. Wang, C. Y.; Liu, C. Y.; Zheng, X. Chen, J.; Shen, T. Colloids Surfaces A: Physicochem. *Eng. Asp.* **1998**, *131*, 271.

47. Chen, K. W.; Ku, Y.; Kuo, Y. L. *Chem. Eng. Technol.* **2007**, *30*, 1242.